This preprint is a peer-reviewed paper accepted for publication in Physics of the Earth and Planetary Interiors on 29 January 2021 (ref PEPI 106659).

to cite the paper

Dumont, S., Silveira, G., Custódio, S., Lopes, F., Le Mouël, J-L., Gouhier, M., Guéhenneux, Y. Response of Fogo volcano (Cape Verde) to lunisolar gravitational forces during the 2014-2015 eruption. Phys. Earth. Planet. Int.,. in press.

Response of Fogo volcano (Cape Verde) to lunisolar gravitational forces during the 2014-2015 eruption

Dumont Stéphanie[1,2,*] Silveira Graça[2,3] Custódio Susana[2,4] Lopes Fernando[5] Le Mouël Jean-Louis[5] Gouhier Mathieu[6] Guéhenneux Yannick[6]

1 Universidade da Beira Interior, Covilhã, Portugal

2 Instituto Dom Luiz (IDL), Faculdade de Ciências, Universidade de Lisboa, Lisboa, Portugal

3 Instituto Superior de Engenharia de Lisboa (ISEL), Lisboa, Portugal ; mdsilveira@fc.ul.pt

4 Faculdade de Ciências, Universidade de Lisboa, Lisboa, Portugal ; sicustodio@fc.ul.pt

5 Institut de Physique du Globe de Paris, Sorbonne Paris cité, Paris, France ; lopesf@ipgp.fr

6 Université Clermont Auvergne, CNRS, IRD, OPGC, Laboratoire Magmas et Volcans, Clermont-Ferrand, France ; M.Gouhier@opgc.fr ; Y.Guehenneux@opgc.fr.

* corresponding author : sdumont@segal.ubi.pt

Abstract

Volcanoes are complex systems that evolve in space and time as a result of their eruptive activity. Volcanic eruptions represent the ultimate expression of a complex interplay between internal and external processes that span across different time scales. Deciphering how internal and external processes interact at the time scale of eruptions may provide key insights on the temporal evolution of eruptions and also help to better evaluate associated volcanic hazards. Studies of the tidal influence on volcanic activity have fallen within this context, although the cause-effect relationship between tides and eruptions is still unclear. In this study, we used Singular Spectrum Analysis to analyze three time-series, namely the seismic tremor, SO_2 emission and lava volume flow rate, which cover the first month of effusive activity at Fogo volcano, Cape Verde, in 2014-2015. We detect 9 tidal periodicities and up to 5 in each time-series ranging from semi-diurnal to fortnightly periods. We show that the movement of magma at crustal depths and at surface as well as gas emission during the effusive eruption are all modulated by lunisolar gravitational forces. We highlight the relevance of the volcano location on Earth, which together with the timing of the eruption, associated with a specific astronomical configuration, result in a specific combination of tides that directly influence the volcano eruptive activity. With this data set, we further investigate the response of Fogo volcano to this external forcing. We show that during the 2014-2015 eruption, Fogo volcano acted as a bandpass filter to quasi-permanent tidal oscillations.

Keywords: 2014-2015 Fogo eruption; earth tides; SSA; seismic tremor; eruptive activity; external forcing

1. Introduction

Periodicities corresponding to lunisolar tides have for long been observed in seismic and volcanic activity (Mauk and Johnston, 1973; Heaton, 1975; Sparks, 1981; Rymer and Brown, 1984; Bodri and Iizuka, 1989; Cigloni et al., 2009; Bredemeyer and Hansteen, 2014; Delorey et al., 2017; Petrosino et al., 2018; Ricco et al., 2019; Varga and Grafarend, 2019). In addition, recent studies have evidenced presence of tides at time scales ranging from a few days to decades, in the polar motion (Lopes et al., 2017), plate motion (Zaccagnino et al., 2020) and even in climate indexes as a response to the temporal evolution of atmospheric pressures (Le Mouël et al., 2019a). At volcanoes, periodic variations have been revealed by various kind of observations such as lava lake height, degassing, micro-seismicity and Long-Period (LP) events, volcanic tremor, ground tilt, temperature of fumarolic fields, energy radiated by lava or strength of eruptive phases (Golombek and Carr, 1978; Berrino et al., 1991; Williams-Jones et al., 2001; Custodio et al., 2003; Sottili et al., 2007; Cigloni et al., 2009; De Lauro et al., 2012, 2013, 2018; Sottilli and Palladino, 2012; Bredemeyer and Hansteen, 2014; Girona et al., 2018; Dinger et al., 2018; Caputo et al., 2020; Dumont et al., 2020; Petrosino et al., 2020). Lunisolar gravitational forces have also been evoked as triggers of volcanic eruptions (Mauk and Johnston, 1973; Dzurizin, 1980; Jentzsch et al. 2001; Dumont et al., 2020).

Different approaches have been considered to demonstrate the correlation between tidal action and variations in volcanic activity, from statistics to spectral or principal component analysis (see examples in Mauk and Johnston, 1973; Patanè et al., 1994; Girona et al., 2018; De Lauro et al., 2013; Dumont et al., 2020). The main and most frequent periodicities detected in time-series acquired at volcanoes are those of the fortnightly, which is induced by the Moon's declination, the semi-diurnal caused by the Sun and lunar elliptic trajectory, as well as the diurnal component which is related to the Sun (Berrino et al., 1991; Custodio et al., 2003; Sottilli and Palladino, 2012; De Lauro et al., 2018; Girona et al., 2018; Le Mouël et al., 2019b). These tidal oscillations are, however, not the only to modulate activity at volcanoes, as suggested by a couple of studies (Sottili and Palladino, 2012; Bredemeyer and Hansteen, 2014; Caputo et al., 2020; Dumont et al., 2020). In spite of all these studies, providing clear evidence on the correlation between processes that occur at very different time scales has proved to be particularly challenging. In addition and beyond the techniques used, the cause-effect relationship between tidal action and volcanic activity has remained elusive (Sparks, 1981; Neuberg, 2000). Tidal stresses and tidal acceleration have been suggested as the main drivers of tidal forcing although tidal stresses are about 3-5 orders of magnitude smaller than tectonic stresses (Mauk and Johnston, 1973; Sparks, 1981), which makes them too low to induce fracturing (McMillan et al., 2019; Dumont et al., 2020). The complexity of volcanic systems, which is mainly due to their eruptive history, composition, internal structure and tectonic setting, also plays an important role on how volcanoes respond to the quasi-permanent tidal oscillations explaining also why all volcanoes do not show a similar sensitivity to Earth tides (Mauk and Johnston, 1973; Dzurizin, 1980). Additionally, the specific positions of volcanoes on the planet, means they are not influenced similarly by the different Earth tides, as the zonal, tesseral and sectorial components of the tidal potential have a specific spatial distribution on Earth (see Jobert and Coulomb, 1973; chapter 18). The spatial distribution and especially the latitudinal position of the different gravitational bodies that interact with the volcano is determinant in the way the tidal potential applies on Earth (Mauk and Johnston, 1973; Hamilton, 1973; Jobert and Coulomb, 1973) .

In this study, we adopted a similar approach to Dumont et al., (2020) and used the Singular Spectrum Analysis to investigate three geophysical time-series, namely the SO_2 emission, lava volume flow rate (VFR) and seismic tremor, spanning the 2014-2015 mix eruption at Fogo volcano, Cape Verde. This eruption started on November 23rd, 2014 and ended on February 8th, after 2.5 months of intense effusive activity (Mata et al., 2017; Richter et al., 2016). The resulting extensive lava field (43.7 x +/- 5.2 10^6 m^3) covered 4.84 km^2 of Chã das Caldeiras and destroyed two villages (Richter et al., 2016; Jenkins et al., 2017). We characterize the lunisolar tidal influence on this dominantly effusive eruption which took place in the Equatorial zone, to further investigate the specific response of Fogo volcano to this permanent external forcing associated with Earth tides.

2. Fogo volcano and the 2014-2015 eruption

Fogo volcano is located on one of the dozen islands composing the Cape Verde archipelago, which lies ~450 km west of Africa, in the North Atlantic (Figure 1). The west-open crescent formed by the islands rises on the top of a 1200 km diameter swell characterized by the largest bathymetric (+ 2 km) and geoid (+ 8m) anomalies in the world which are thought to result from an upwelling mantle plume (Courtney and White, 1986; Grevemeyer, 1999; Carvalho et al., 2019). The rise of the Cape Verde islands initiated early Miocene (~22 Ma) but most of the islands formed in the last 16 Ma (Holm et al., 2008). Mantle channeling has been proposed to explain the position of islands along three main groups: northwest, east and southwest (Holm et al., 2008). Fogo belongs to the latest group and is one of the most recent islands formed in the Quaternary (Ramalho et al., 2010). Fogo and its western neighboring island, Brava, are the center of the present-day seismic and magmatic activity of the whole archipelago (Silva et al., 1999; Amelung and Day, 2002; Custodio et al., 2003; Dionis et al., 2015; Eisele et al., 2015; González et al., 2015; Faria and Fonseca, 2014; Vales et al., 2014; Leva et al., 2019).

Fogo island is characterized by steep slopes topped by a 9 km diameter horseshoe-shaped caldera, Chã das Caldeiras. The geometry of the 1-km high caldera wall evidences past collapse events whose nature and origin are still debated nowadays although the risk of associated tsunami is well recognized. One catastrophic event was identified at ~65 to 84 kyrs but it may not be the only one (Day et al., 1999; Ramalho et al., 2015; Barrett et al., 2019). Since the last flank collapse, the volcanic activity has been focused on the Fogo volcano, after which the island was renamed, a stratovolcano rising at 2829 m above sea level nearby the center of the caldera (Figure 1). The Fogo volcano is considered as one of the most active volcanoes in the Atlantic, with 28 eruptions since the settlement in the early 15th century (Faria, 2010). The repose period between eruptions has changed over the last 600 years with eruptions every ~60 years on average between 1400 and 1680, one every ~5 years between 1750 and 1875 and one every ~20 years since the last century (Faria, 2010). Tephrostratigraphic analyses of off-shore tephra revealed a past and highly explosive eruptive activity of Fogo estimated to occur every ~3000 years during the last 150 kyrs (Eisele et al., 2015). The last summit eruption occurred in 1785 and since then most eruptions took place on volcano flanks (Faria, 2010; Amelung and Day, 2002; González et al., 2015). The last three eruptions (1951, 1995, 2014-15) produced extensive lava flows that threatened local populations and caused the total destruction of two villages in 2014-15 (Richter et al., 2016; Jenkins et al., 2017).

The last eruption of Fogo started on 23 November 2014 and lasted 77 days, ending on 7 February 2015. The eruptive fissure opened with a violent explosion a few hundred meters away from the 1995 cinder cone. It was initially formed by 6-7 individual vents that reduced to 3 over the course of the eruption. Lava fountains and Strombolian explosions mainly composed this volcanic activity punctuated by stronger explosions and ash plume emissions (Mata et al., 2017; Calvari et al., 2018). Remote-sensing imagery revealed a mean effusion rate of 6.8 $m^3.s^{-1}$, with a peak of ~24-27 m^3s^{-1} achieved on 24 November and very low discharge rates after late December (Cappello et al., 2016; Calvari et al., 2018). The new lava field covered an area of ~5.42 km^2 at the end of the eruption, corresponding to a total volume of 9.6-18.2 10^6 m^3 (Bagnardi et al., 2016; Richter et al., 2016). The magma erupted during this eruption was mainly alkaline with some evolved compositions, e.g. tephrites to phonotephrites. The Nb/U ratios, lower than those of the two previous eruptions, were interpreted as an expression of small-scale mantle heterogeneity (Mata et al., 2017).

3. Data and Methods

3.1 Retrieval of lava and SO_2 emissions

Lava Volume Flow Rate (VFR) and SO_2 vertical column densities (VCD) have been retrieved together from the HOTVOLC system. HOTVOLC is a Web-GIS volcano monitoring system using SEVIRI (Spinning Enhanced Visible and Infrared Imager) sensor on-board Meteosat geostationary satellite (https://hotvolc.opgc.fr) and developed at the OPGC (Observatoire de Physique du Globe de Clermont-Ferrand) in 2009 (Gouhier et al., 2016). The spectral bands of the SEVIRI sensor allow us to simultaneously characterize volcanic ash (Guéhenneux et al., 2015), sulfur dioxide (Gauthier et al., 2016; Gouhier and Paris, 2019), and lava flow emissions (Gouhier et al., 2012; Gouhier et al., 2016; Thivet et al., 2020). It is designed for the real-time monitoring of ~50 active volcanoes, including Fogo volcano and provides high value-added products at the frequency of 1 image / 15 min with a pixel resolution of 3 km × 3 km at nadir. For this study, 7488 multispectral IR images have been processed, covering the whole eruption duration.

Lava effusion rates have been estimated using instantaneous lava volumes, calculated from infrared techniques. This method lies on the mass conservation principle and benefits from a rapid succession of images obtained using geostationary satellites. The physical principle is as follows: the pixel-integrated thermal anomaly measured at a given instant is the balance of contributions related to (i) hot lava material newly emplaced (at time *t*) and (ii) cooling lava material previously emplaced (at time *t-1*). This problem can be addressed using the mass conservation principle following the differential equation:

$$\frac{dV(t)}{dt} = Q(t) - kV(t)$$

V is the total volume of lava in a given image, Q is the lava volume flow rate (i.e., source term) and $-kV$ is the loss term with k representing the lava cooling rate (s^{-1}). Note that satellite observations provide discrete time series, to obtain Q we thus solve analytically the above differential equation with Δt being the time interval between two consecutive images such that:

$$Q(t) = k\,\frac{V_i - V_{i-1}e^{-k\Delta t}}{1 - e^{-k\Delta t}}$$

The cooling rate k is often expressed as $k=1/\tau$, where τ is the lava e-cooling time. This method, referred to as the Volume Flow Rate (VFR) method, allows the calculation of quasi-instantaneous lava effusion rates (in m^3/s). The quantification of instantaneous lava effusion rates is essential as it strongly controls the lava front speed and flow area. Moreover, the short-term evolution of lava effusion rate traduces eruptive dynamics changes from shallow depth to the surface.

Volcanic SO_2 emissions have long been characterized from thermal infrared sensors using absorption features of either the 8.7-µm waveband (e.g., Watson et al., 2004) or the 7.3-µm waveband (Prata et al., 2003). The retrieval scheme used here follows from Realmuto et al., (1994), where the SO_2 column abundance, referred to as VCD, is estimated from the 8.7-µm waveband using a linear regression derived from a least square fitting procedure between sensor measurements (i.e., SEVIRI) and simulated radiances using the Modtran radiative transfer model. VCD are usually expressed in Dobson Unit (DU) for SO_2 abundance. One Dobson Unit corresponds to 2.69×10^{20} molecules per square meter, i.e., 2.86×10^{-5} kg/m^2. Finally, we provide here the maximum SO_2 VCD (in DU) for each image in the form of a time series over the whole eruption duration.

3.2 Seismic tremor

The amplitude of seismic tremor was quantified using data collected by a temporary network of seven broadband seismic stations (Figure 1), which were quickly deployed after the eruption began. This network operated for about one month and a half, between November 28, 2014 and January 15, 2015. All stations were equipped with CMG6TD sensors (30s to 100 Hz) and recorded continuously at a sample rate of 100 Hz.

Continuous seismic data were initially instrument-corrected and converted to true ground velocity, after demeaning, detrending and tapering. Data were then filtered between 1 and 4 Hz, the frequency band typically associated to volcanic tremor. In order to assess the evolution of the amplitudes of seismic tremor, we computed the Root Median Square (RMeS) of the band-pass filtered continuous seismic records as in Eibl et al., (2017). RMeS is calculated as $\sqrt{Median(y_i^2,\dots,y_f^2)}$, where the median is calculated based on the squared amplitudes of seismic data recorded in each 15-min sliding window (y_i and y_f are the initial and final seismic amplitudes in each window). We use a 50% overlap between neighbor windows. For this study, we considered the seismic tremor observed at station FCVT (Covatina), which is the station closest to the eruptive fissure (< 5 km, Figure 1).

3.3 Length-of-Day (l.o.d.) and sea level measurements

The length-of-day (l.o.d.) is an astronomical measure of the Earth's rotation velocity. It is one of the Earth orientation parameters, measured from the combination of Very Long Baseline Radio Interferometry (VLBI), Satellite Laser ranging (LSR) with Doppler Orbitography and Radio positioning Integrated by Satellite (DORIS) techniques (Bizouard et al., 2019). For this study, we used the EOP14C04 data set provided by the International Earth Rotation Service (https://www.iers.org/IERS/EN/DataProducts/EarthOrientationData/eop.html, IERS, Paris, France). Both regular and irregular l.o.d. variations have been evidenced at several time scales, from a few days to decades (Guinot, 1973; Lambeck et al., 2005; Ray and Erofeeva, 2014; Le Mouël et al., 2019b). Decadal fluctuations have been attributed to core/mantle interaction and their dynamics, while rapid variations to external forcings, including atmosphere dynamics and Earth tides (Lambeck et al., 2005). On the time scale of a few months, l.o.d. variations do not exceed 2 ms.

We complement l.o.d daily measurements with those of sea level in order to capture daily and sub-daily tides at Cape-Verdian latitudes. For this purpose, we used hourly data from the tide gauge station Palmeira (16.75ºN, -22.983333ºE), located on Sal island (Cape Verde, Figure 1b). The data are acquired and validated by the UH Sea Level Center via the Permanent Service for mean sea level platform (Holgate et al., 2013; PSMSL, 2019).

3.4 Singular Spectrum Analysis

We analyzed the five geophysical time-series using the Singular Spectrum Analysis (SSA). SSA is a non-parametric time-series analysis technique based on two steps, a decomposition and a reconstruction allowing to identify trends, periodic or quasi-periodic components and noise in any signal as independent and physical components (Vautard and Ghil, 1992; Golyandina and Zhigljavsky, 2013). The first step consists in building a diagonal auto-correlation matrix corresponding in our case to a Hankel matrix. To do so, lagged copies representing segments of length L of the time-series are embedded to create a L x K matrix, with K = N -L +1 and N the length of the time-series. This analysis is sensitive to the dimensions of the Hankel matrix as smaller L will make the analysis closer to fractal, while larger L will result in reconstructions very similar to the original time-series. The Hankel matrix, H, is then decomposed using the Singular Value Decomposition (SVD) algorithm such as follows:

$$\mathrm{H} = \sum_{i=1} \sqrt{\lambda_i} U_i V_i^T$$

Where $\sqrt{\lambda_i}$ is the matrix containing the singular values, U_i and V_i the left and right matrices of the orthogonal singular vectors. One of the advantages of the SVD is that it ranks the singular values in the descending order of the energies and therefore their contribution to the original time-series as well. This way, a signal whose mean value is non-null is characterized by a trend that will appear in the first eigenvalues. The eigen tiplets (eigenvalues and eigenvectors) associated with eigenvalues of similar magnitude may be grouped. In the case of a perfect oscillation, SSA produces two identical eigenvalues called Hilbert pair. Thus, different components of the time-series, e.g the trend, (pseudo) cycles and noise can be identified and reconstructed by gathering small groups of eigenvalues having very close contributions. Noise is usually of small amplitude and represented by small eigenvalues. Identifying the eigenvalues of interest allows to filter non-linearly the original signal by truncating the SVD using the selected eigenvalues.

In the present study, we focus on components whose periods were very similar to that of known Earth tides and whose separability with neighboring components was sufficient to properly identify individual tidal components. The uncertainties on each identified period as later presented in Figures 3 & 4 and Table 1, were estimated using the half-width of their peaks at half-height, similarly to Le Mouël et al. (2019)a,b and Dumont et al. (2020). More details on the method, its application and discussion on critical aspects of SSA can be found in Lopes et al. (2017) and Le Mouël et al., (2019a,b; 2020).

The significant cloud cover associated with lower lava emissions from mid-December to February 2015 originated important gaps in the estimation of lava VFR and SO_2 VCD measured from SEVIRI data. SSA was therefore applied from 23th November to 22 December 2014, covering a 30-days interval, for the lava VFR and SO_2 time-series. For similar reasons, we analyzed the seismic tremor detected at FCVT station for the period starting on 30th November and ending on 26 December 2014 (Figure 2). The l.o.d and sea level time-series representing reference data sets for identifying tidal periodicities, were analyzed using SSA for the whole eruption duration (23 November 2014 – 8 February 2015).

3.5 Tidal potential calculation

The tidal potential W (see Jobert and Coulomb, 1973, chapter 18) is given by the following expression : $W = \frac{G M'}{D} \Sigma_{n=2}^{\infty} (\frac{R}{D})^n P_n (\cos (z))$, where G represents the Newton gravitational constant, M' the mass of the celestial body, e.g that of the Sun or the Moon; D its distance to the Earth; R, the Earth's radius and P_n the Legendre's polynomial function of the cosine relating to the celestial body position. W may be decomposed in a sum of spherical harmonics. It is usually reduced to its first term (n=2) when focusing on the strongest tides induced by the gravitational effect of Moon and the Sun, the distances between the other planets of the solar system and the Earth being tremendous. W_2 may be described as follows (Jobert and Coulomb, 1973):

$$W_2 = (G M' R^2) (P_2 \cos Z) / D^3$$

with Z, the zenithal distance of the celestial body at the observation site on Earth and P_2 the Legendre's polynomial of second order (see graphic Figure 5a). D and Z vary in time for both the Sun and the Moon. D time-series are freely accessible from the Institut de Mécanique Céleste et de calcul des Éphémérides website (http://vo.imcce.fr/webservices/miriade/?forms). The zenithal distance Z, may be calculated using the right ascension (H) and the declination (δ) of the Moon/Sun that is given by the ephemeris, as well as the longitude (φ) and latitude (θ) of the observation point. It follows that, at about one common factor given by G M' R^2/D^3, the tidal potential W_2 is composed of three main tides, the zonal ($W_{2,0}$), tesseral ($W_{2,1}$) and sectorial ($W_{2,2}$) components which are characterized by different periods and specific spatial distribution. They can be expressed as follows (Jobert and Coulomb, 1973) :

$$W_{20}(\cos Z) = 0.5(3\cos^2\theta - 1) \quad * \; 0.5(3\cos^2\delta - 1)$$

$$W_{21}(\cos Z) = 3\sin\theta\cos\theta \quad * \; 3\sin\delta\cos\delta \quad * \; \cos(H - \phi)$$

$$W_{22}(\cos Z) = 3\cos^2\theta \quad * \; 3\cos^2\delta \quad * \; \cos 2(H - \phi)$$

With these equations, it is clear that the spatial configuration of the Moon and Sun with respect to the observation site at a specific time will define the magnitude and phase shift of the tidal potential experienced at the observation site.

4. Results

MSG-SEVIRI satellite images reveal a maximum of lava VFR and SO_2 VCD detected between 1 and 2 days respectively, after the onset of the eruption (Figure 2). Although the seismic tremor data does not cover the first week of the eruption, it still shows significant variations with a maximum reached on 3rd December, followed by an overall slow decay. A stronger decline is observed for the SO_2 VCD that drops by half in about a week and then slightly varies around an index value of 8 for the rest of the eruption. The lava VFR shows a different behavior with a strong emission of lava including large variations up to mid-December, reported as cycles by Cappello et al., (2016). For this time interval, the l.o.d. shows regular variations of the order of 0.5 ms (Figure 2), except in the first week of January 2015 where a drop exceeds 0.8 ms. The sea level time-series show larger variations of the order of 140-160 cm on average, with an overall trend similar to that of the l.o.d (Figure 2). Both l.o.d. and sea level variations are governed by clear periodic oscillations that span different time scales as illustrated by their spectra (Figure 3a). Normalized spectra already reveal common periodicities in the three volcanological time-series of the first month of the eruption what we will further explore next.

We analyzed the trends and (pseudo-) periods that compose the lava VFR, SO_2 and seismic tremor time-series by considering up to 20-25 eigenvalues for each SSA decomposition (Figure 3b). We thus identified 9 periods corresponding to the main components of the Earth tides, ranging from 0.5 to ~15 days and an additional ~4.5-day period (see Table 1). The presence of this ~4.5-day period oscillation in two of the three geophysical data series, e.g SO_2, lava VFR and l.o.d. likely reflects a common origin, what we interpret as a harmonic of a longer lunisolar or lunar tide. Thus, we clearly detected 5 tidal components in the seismic tremor, 5 in the SO_2 time-series and 4 in the lava VFR, which match well those identified in the l.o.d. or sea level data (Table 1). One can note the clear dominance of lunar tidal periods over those of solar origin. For each volcanological time-series, we combined these tidal components with the trends that are usually associated with volcanic processes (see Dumont et al., 2020) to reconstruct the original time-series (Figure 3c). We only excluded the solar semi-diurnal component (S2) extracted from the lava VFR data, as it is not a pure tide but rather a tide-induced thermal effect on the atmosphere. Indeed, the absorption of solar radiations produces water vapor that circulates and condensates in the atmosphere, releasing thus latent heat during the water vapor cycle at harmonics of a solar day (Hagan and Forbes, 2002). These trends and lunisolar tidal periods that we identified allow to reproduce most variations as illustrated with the Figure 3c. More precisely, we are able to reconstruct up to 96.2% of the SO_2 time-series, 85.6 % of the seismic tremor and 53.1% of the lava VFR. Next, we present some of the waveforms associated with the tidal components identified in the volcanological time-series.

Figure 4 presents two of the three long tides extracted in the seismic tremor, lava VFR and SO_2 time-series. The seismic tremor displays two out of these three long-period tides (Table 1). The component with a period of 14.9 +/- 5.8 days, likely corresponds to the lunisolar fortnightly tide, being possibly caused either by the oscillations of the Moon declination, e.g Mf with a 13.6-days period, or reflecting half of the synodic lunar month, e.g MSf with a 14.7-days period. Despite a relatively large uncertainty, this tidal component identified in the seismic tremor appears clearly in phase opposition with that of the l.o.d (Figure 4). The lunar constituent Mt with a ~7.0-days period, is in-phase for both seismic tremor and lava VFR. For both components, the amplitude increases up to ~10th December, after which it decreases, a pattern that is more pronounced for the seismic tremor. Figure 4 also shows shorter periods with the example of one diurnal and one semi-diurnal. Four tidal constituents with near diurnal periods are detected in the volcanological time-series, namely 2Q1, M1, P1 and K1 (Table 1). The P1 tidal component detected in the lava VFR may possibly reflect the sensitivity of the mid-wave infrared band (3.9 μm) to solar diurnal tides, even though data processing includes a step to remove it. Except for the solar component P1 detected only in the lava VFR, the three other near-diurnal constituents were detected in both the SO_2 and seismic tremor as well as in the sea level data. The two components of the larger elliptic diurnal or 2Q1 tide are mainly in phase opposition and show a strong attenuation starting early December for the SO_2 and after 21st December for the seismic tremor (Figure 4). Although centered on 1.17 days, the SO_2 component of the 2Q1 tide has an uncertainty that is wide enough to allow it to be interpreted as Q1 or M1. The lunar elliptic semi-diurnal components (N_2, first or second order, Table 1) in the SO_2 and seismic tremor time-series also attenuate over time. They are decaying at a very similar rates, although they are in quadrature after 1st December (Figure 4). One can note that the amplitude of the SO_2 and seismic tremor components are larger when those of the sea-level are smaller.

5. Discussion

The Singular Spectrum Analysis applied to three geophysical time-series acquired during the 2.5-month Fogo eruption provides a new evidence of the influence of lunisolar gravitational forces on effusive eruptions. We identified between 4 and 5 tidal periodicities in the SO_2, lava VFR and seismic tremor time-series with periods ranging from semi-diurnal to fortnightly (Table 1, Figure 4). These results confirm and complement the observations made by Dumont et al. (2020) showing that the movements of magmatic fluids at volcanoes (melt, erupted magma and gas emission) are not modulated by one but rather by a combination of several earth tides as it had also been suggested by Sottili and Palladino (2012) and Bredemeyer and Hansteen (2014). In addition, this analysis confirms the predominant influence of lunar tides over lunisolar ones on volcanic processes, e.g De Lauro et al., (2013).

It is interesting to note that this analysis detected many more tides of short periods (Table 1) than those that had been detected for Holuhraun eruption that was ongoing before the onset and after the termination of Fogo eruption (Dumont et al., 2020). This observation might however be biased by the time interval considered by this study, i.e. ~1 month instead of the ~2.5 months of the whole eruptive period at Fogo, preventing the detection of longer tides. Another way to address the differences of tides present in the co-eruptive geophysical time-series in Iceland and Cape Verde is to consider the components identified in each time-series and the rank of their associated eigenvalues (Figure 3b). The longest tide we identified for Fogo eruption, the fortnightly, appears in the seismic tremor only as fourth component, after the trend, a 2.4-day period and a 7.9-days period oscillations. This contribution of Mf/MSf to the seismic tremor time-series at Fogo is smaller than those in both the seismic tremor and radiated power for the Holuhraun eruption (see the values of the normalized eigenvalues, ~0.05 versus ~0.07, Figures 3 this study and Dumont et al., 2020), that are also systematically ranked second after the trend. Similarly, the 9.4 day-period or Mtm tide, was only detected in the SO_2 data at Fogo, where it appears in tenth position (Figure 3b). This tide was ranked higher in the seismic tremor of the Holuhraun eruption, in sixth position, associated with higher normalized eigenvalues (Dumont et al., 2020). The semi-diurnal and diurnal oscillations detected in the three geophysical time-series during Fogo eruption are more numerous, with ranks between 4 and 25 (Figure 3b). This comparison suggests that at low latitude, longer tides are generally weaker than at higher latitudes and have also a stronger contribution in parameters related to magma propagation, as shown by VFR and seismic tremor time-series, rather than those related to gas fluxes. This variety of lunar, solar and lunisolar tides was not detected for the Icelandic data sets. It is important to remind that the tidal contributions we captured for Fogo eruption are of first-order as we could only analyze slightly less than half of the eruption duration.

Let us now further explore the contribution of the fortnightly component at these two eruption sites, Fogo and Holuhraun, by calculating the tidal potential. The fortnightly periodicity Mf is related to variations of the Moon declination which are mainly related to the zonal component of the tidal potential, $W_{2,0}$. We estimated $W_{2,0}$ between late November and late December 2014 at the Icelandic and Cape-Verdian eruption sites (Figure 5). This calculation clearly shows that this tide is stronger at higher latitude than nearby the Equator explaining why it was more easily and systematically detected in all geophysical parameters for the Holuhraun eruption than for Fogo (Dumont et al., 2020). Moreover, because of its location in the Equatorial band, Fogo volcano is more sensitive to the solar tides than Iceland, and even more so towards the end of the year when the Earth is closest to the Sun. Altogether, these observations suggest that the influence that tides have on volcanic activity is a result of the combination of tides that is specific to the volcano location on Earth and also to the timing of the eruption which is associated with a specific astronomical configuration. We also note that the onset of Fogo eruption dated to the 23rd November 2014 occurred only one day after a syzygy (new Moon). Such a short timing have been evoked to suggest the tidal influence on the triggering mechanisms of volcanic eruptions (Mauk and Johnston, 1973; Dzurisin, 1980; Jentzsch et al. 2001; Sottili and Palladino, 2012; Dumont et al., 2020).

The three time-series that we analyzed for Fogo eruption provide insights on 1) the movement of volatile-bearing magma from depth to surface, as documented by the seismic tremor, 2) the emission of gas once the magma erupted, as evidenced with the SO_2 emissions and 3) the movement of magma at Earth's surface as illustrated with the lava VFR. Although tidal waves do not require a medium to propagate as they deform the space-time geometry, the waveforms associated with the tidal components that we extracted from the volcanological time-series seem to show some features related to their propagation medium. Actually, attenuation of the waveforms is systematically observed for the seismic tremor and the SO_2 emission in particular, but (almost) not observed in the lava VFR (Figure 4). Indeed, the lava field growth was characterized at Fogo by early formation of lava tubes that started early December for the second and main flow and earlier for the first and short flow (Calvari et al., 2018). The efficient thermal insulation of lava tubes (Keszthelyi, 1995) as well as the steady magma supply rate (Calvari et al., 2018) could explain this reduced attenuation of lava VFR waveforms. The seismic tremor is thought to be associated with movement of fluids at subsurface and has often be correlated with the intensity of volcanic activity (Chouet, 1985; Eibl et al., 2017 and therein references). The attenuation observed for the tidal components of the seismic tremor may represent the decrease of the eruption vigor. However, the ascent of a hot and multi-phase melt in a very heterogeneous medium (fractured and temperature-eroded) towards the surface at rates that are likely varying over the eruption duration, may also contribute to attenuate differently the various tidal components of the seismic tremor. Finally, the strong attenuation detected in the gas emissions is likely due to the dispersive nature of the atmosphere.

All these observations suggest that volcano's response to Earth's tides is highly dependent on the nature of the magma erupted, as well as on the structure of the internal plumbing system and on tectonic setting, as also previously suggested by various studies (Mauk and Jonhston, 1973; Dzurisin, 1980; Sparks, 1981; Petrosino et al., 2020). To further characterize the volcano's response to this quasi-permanent external forcing, let's consider x as the tidal potential and y as the geophysical parameters influenced by earth tides and recorded during an eruption (e.g. volcanic tremor, gas release, lava emission...) and h, the impulse response of the volcano corresponding to all geochemical-physical processes characterizing the volcano activity. Using filter theory, we can describe the impulse response of the volcano as follows:

$$y(t) = (h * x)(t)$$

In the Fourier space, this equation corresponds to a simple product: $Y(f) = H(f).X(f)$

Y and X are the Fourier transforms of y and x respectively and H corresponds to the transfer function of the volcano, with f, the frequency. SSA allowed us to extract and identify the pseudo-oscillations of tidal origin in the three geophysical time-series. It is therefore possible to reconstruct H for all the identified periodicities. The tidal potential x for the identified tidal periods is known (Guinot, 1973; Ray et al., 2014). By representing the amplitude and phase of each tidal period extracted from the seismic tremor, lava VFR and SO_2 as a function of their frequencies, we can characterize the pulse response of Fogo volcano. Figure 6 shows that Fogo volcano seems to respond as a bandpass filter (~0.1-0.85 $days^{-1}$) to the external tidal forcing, being more sensitive to tidal periods slightly longer than 24 h such as those of Q1, and up to longer tides with periods up to ~9 days (Table 1), including Msp, Mt, Mtm tides. We suggest that the band width of this filter is likely related to the internal structure of the volcano, its chemistry and geodynamical setting, as suggested by Mauk and Jonhston (1973), Dzurisin (1980) or De Lauro et al., (2018). Further investigations on such response of volcanoes to external forcing could provide a new way to address the interplay between internal and external processes that influence magmatic and volcanic activity.

6. Conclusion

Our study focuses on the 2014-2015 eruption of the Fogo volcano, Cape Verde. We analyze three co-eruptive geophysical time-series, namely the seismic tremor, SO_2 emissions and lava volume flow rate (VFR), using the Singular Spectrum Analysis (SSA). By considering the first month of the eruptive activity, we were able to identify between 4 and 5 different tidal periods in each of these volcanological time-series, ranging from semi-diurnal to fortnightly periods. These results clearly show a predominant influence of lunar tides, although solar and lunisolar tidal periods were also detected. The retrieval of the waveforms associated with the tidal components extracted from the different time-series, reveals a stronger attenuation for the tidal components of the SO_2 and seismic tremor. By comparing these observations to those obtained for Holuhraun eruption (Iceland) (Dumont et al., 2020), we illustrate that the forcing of tides upon volcanic activity is a result of both the volcano location on Earth and of the timing of the eruption, which corresponds to a specific astronomical configuration. Finally, using filter theory we demonstrate that Fogo volcano responds as a bandpass filter to the quasi-permanent tidal oscillations.

Acknowledgment

The authors would like to thank E.P.S Eibl for fruitful discussion on data processing and João Fonseca for making possible the seismic mission to Fogo and its contribution to the FIRE project. The authors also thank two anonymous reviewers and Mark Jellinek, for editorial handling. SD would like to thank the Fundação para a Ciência e a Tecnologia (FCT) for his financial support through the postdoctoral grant (SFRH/BPD/17714/2016), as part of Human Capital Operating Programme (POCH) and the European Union. This work was also supported by FCT through the project FIRE (PTDC/GEO-GEO/1123/2014) and the Instituto Dom Luiz, IDL (UIDB/50019/2020). The deployment of a temporary seismic network in Fogo island was supported by the Collaboratory for Geosciences (C4G), a distributed research infrastructure of the Portuguese Roadmap (POCI-01-0145-FEDER-022151).

Authors' contributions

SD: Formal analysis; Visualization; Writing - original draft;

GS, SC and MG: Formal analysis; reviewing and editing;

FL and JLLM: Conceptualization; Methodology; editing;

YG: Formal analysis;

Data Availability

The SO_2 emission and lava volume flow rate (VFR) time-series are available from the HOTVOLC platform (https://hotvolc.opgc.fr). The l.o.d time-series is freely accessible as part of the EOP14C04 data set provided by the International Earth Rotation Service (https://www.iers.org/IERS/EN/DataProducts/EarthOrientationData/eop.html, IERS, Paris, France) as well as that of the sea level, accessible from Permanent Service for mean sea level platform (PSML, 2019). The seismic tremor data is available upon request.

REFERENCES

Amelung, F., & Day, S. (2002). InSAR observations of the 1995 Fogo, Cape Verde, eruption: Implications for the effects of collapse events upon island volcanoes. *Geophys. Res. Lett.*, *29*(12), 47-1.

Bagnardi, M., González, P. J., & Hooper, A. (2016). High resolution digital elevation model from tri-stereo Pleiades-1 satellite imagery for lava flow volume estimates at Fogo Volcano. *Geophys. Res. Lett.*, *43*(12), 6267-6275.

Barrett, R., et al. (2019). Revisiting the tsunamigenic volcanic flank-collapse of Fogo Island in the Cape Verdes, offshore West Africa. *Geol. Soc. (Lond), Spe. Publ.*, *500*. https://doi.org/10.1144/SP500-2019-187

Berrino, G., & Corrado, G. (1991). Tidal signal in the recent dynamics of Campi Flegrei caldera (Italy). *J. Volcanol. Geotherm. Res.*, *48*(1-2), 93-101.

Bizouard, C., et al. (2019). The IERS EOP 14C04 solution for Earth orientation parameters consistent with ITRF 2014. *J. Geod*. 93, 621–633. https://doi.org/10.1007/s00190-018-1186-3

Bodri, B., & Iizuka, S., On the correlation between Earth tides and microseismic activity. *Phys. Earth Planet. Inter.*, 55(1-2), 126-134, 1989. https://doi.org/10.1016/0031-9201(89)90238-0

Bredemeyer, S., & Hansteen, T. H. (2014). Synchronous degassing patterns of the neighbouring volcanoes Llaima and Villarrica in south-central Chile: the influence of tidal forces. *Int. J. Earth Sci.*, 103(7), 1999-2012. https://doi .org /10 .1007 /s00531 -014 -1037 -2.

Cappello, A., et al. (2016). Lava flow hazard modeling during the 2014–2015 Fogo eruption, Cape Verde. *J. Geophys. Res., Solid Earth*, *121*(4), 2290-2303.

Calvari, S., et al. (2018). Satellite and Ground Remote Sensing Techniques to Trace the Hidden Growth of a Lava Flow Field: The 2014–2015 Effusive Eruption at Fogo Volcano (Cape Verde). *Remote Sensing*, *10*(7), 1115. https://doi.org/10.3390/rs10071115

Caputo, T., et al. (2020). Spectral analysis of ground thermal image temperatures: what we are learning at Solfatara volcano (Italy). Advances in Geosciences, 52, 55-65.

Carvalho, J., et al. (2019). Evidence for high temperature in the upper mantle beneath Cape Verde archipelago from Rayleigh-wave phase-velocity measurements. *Tectonophysics*, *770*, 228225. https://doi.org/10.1016/j.tecto.2019.228225

Chouet, B. (1985). Excitation of a buried magmatic pipe: a seismic source model for volcanic tremor. J. Geophys. Res. 90, 1881–1893.

Cigolini, C., et al. (2009). Radon surveys and real-time monitoring at Stromboli volcano: Influence of soil temperature, atmospheric pressure and tidal forces on 222Rn degassing. J.Volcanol. Geotherm. Res., 184(3-4), 381-388.

Courtney, R. C., & White, R. S. (1986). Anomalous heat flow and geoid across the Cape Verde Rise: evidence for dynamic support from a thermal plume in the mantle. *Geophys. J. Int.*, 87(3), 815-867. https://doi.org/10.1111/j.1365-246X.1986.tb01973.x

Custodio, S. I., et al. (2003) Tidal modulation of seismic noise and volcanic tremor. *Geophys. Res. Lett*, *30*(15). https://doi .org /10 .1029 /2003GL016991.

Day, S. J., et al. (1999). A past giant lateral collapse and present-day flank instability of Fogo, Cape Verde Islands. *J. Volcanol. Geotherm. Res.*, *94*(1-4), 191-218. https://doi.org/10.1016/S0377-0273(99)00103-1

De Lauro, E., et al. (2012). Study on the Long-Period source mechanism at Campi Flegrei (Italy) by a multi-parametric analysis. *Phys. Earth Planet. Inter.*, 206-207, 16-30. https://doi .org /10.1016/j.pepi.2012.06.006

De Lauro, E., et al. (2013). Synchronization between tides and sustained oscillations of the hydrothermal system of Campi Flegrei (Italy). *Geoch., Geophys., Geosyst.*, *14*(8), 2628-2637. https://doi.org/10.1002/ggge.20149

De Lauro, E., Petrosino, S., Ricco, C., Aquino, I., & Falanga, M. (2018). Medium and long period ground oscillatory pattern inferred by borehole tiltmetric data: New perspectives for the Campi Flegrei caldera crustal dynamics. Earth Planet. Scie. Lett., 504, 21-29.

Delorey, A. A., et al. (2017). Tidal triggering of earthquakes suggests poroelastic behavior on the San Andreas Fault. *Earth Planet. Sci. Lett.*, *460*, 164-170. https://doi.org/10.1016/j.epsl.2016.12.014

Dinger, F., et al. (2018). Periodicity in the BrO/SO2 molar ratios in the volcanic gas plume of Cotopaxi and its correlation with the Earth tides during the eruption in 2015. *Solid Earth*, *9*, 247-266. https://doi .org /10 .5194 /se -2017 -89

Dionis, S. M., Pérez, N. M., Hernández, P. A., Melián, G., Rodríguez, F., Padrón, E., ... & Bandomo, Z. (2015). Diffuse CO2 degassing and volcanic activity at Cape Verde islands, West Africa. *Earth, Planets and Space*, *67*(1), 48. https://doi.org/10.1186/s40623-015-0219-x

Dumont, S., et al. (2020). The dynamics of a long-lasting effusive eruption modulated by Earth tides. *Earth Planet. Sci. Lett.,* 536, 116145. https://doi.org/10.1016/j.epsl.2020.116145

Dzurizin, D. Influence of fortnightly earth tides at Kilauea volcano, Hawaii. *Geophys. Res. Lett.*, *7*(11), 925-928, 1980. https://doi .org /10 .1029 /GL007i011p00925

Eibl, E. P., et al. (2017). Tremor-rich shallow dyke formation followed by silent magma flow at Bárðarbunga in Iceland. *Nat. Geosci.*, *10*(4), 299-304. https://doi .org /10 .1038 /ngeo2906

Eisele, S., et al. (2015). Pleistocene to Holocene offshore tephrostratigraphy of highly explosive eruptions from the southwestern Cape Verde Archipelago. *Marine Geol.*, *369*, 233-250. https://doi.org/10.1016/j.margeo.2015.09.006

Faria B, 2010. Monitorização Geofísica do Vulcão do Fogo e Níveis de Alerta. Ph.D thesis. Universidade Técnica de Lisboa. In, Portuguese.

Faria, B., & Fonseca, J. F. B. D. (2014). Investigating volcanic hazard in Cape Verde Islands through geophysical monitoring: network description and first results. *Nat. Hazards Earth Syst.,* 14(2), 485. https://doi .org /10.5194/nhess-14-485-2014

Gauthier, P. J., et al. (2016). Elevated gas flux and trace metal degassing from the 2014–2015 fissure eruption at the Bárðarbunga volcanic system, Iceland. *J. Geophys. Res., Solid Earth*, *121*(3), 1610-1630. https://doi.org/10.1002/2015JB012111

Girona, T., et al. (2018). Sensitivity to lunar cycles prior to the 2007 eruption of Ruapehu volcano. *Scientific reports*, *8*(1), 1476. ttps://doi .org /10.1038/s41598-018-19307-z

Golombek, M. P., & Carr, M. J. (1978). Tidal triggering of seismic and volcanic phenomena during the 1879–1880 eruption of Islas Quemadas volcano in El Salvador, Central America. *J. Volcanol. Geotherm. Res.*, 3(3-4), 299-307.

Golyandina, N., & Zhigljavsky, A. (2013). Singular spectrum analysis for time series. Heidelberg, New York, Dordrecht, London: Springer Briefs in Statistics 119pp. https://doi.org/10.1007/978-3-642-34913-3

Gouhier, M., & Paris, R. (2019). SO2 and tephra emissions during the December 22, 2018 Anak Krakatau eruption. *Volcanica*, *2*(2), 91-103.

Gouhier M., et al. (2016). HOTVOLC: a web-based monitoring system for volcanic hot spots. *Geol. Soci. (Lond.), Spec. Public.*, 426, SP426-31. https://doi.org/10.1144/SP426.31

Gouhier, M., et al. (2012). Lava discharge during Etna's January 2011 fire fountain tracked using MSG-SEVIRI. *Bull. Volcanol.*, *74*(4), 787-793.

González, P. J., et al. (2015). The 2014–2015 eruption of Fogo volcano: Geodetic modeling of Sentinel-1 TOPS interferometry. *Geophys. Res. Lett.*, *42*(21), 9239-9246. https://doi.org/10.1002/2015GL066003

Grevemeyer, I. (1999). Isostatic geoid anomalies over mid-plate swells in the Central North Atlantic. *J. Geod.*, 28(1), 41-50.

Guéhenneux, Y., et al. (2015). Improved space borne detection of volcanic ash for real-time monitoring using 3-Band method. *J. Volcanol. Geotherm. Res.*, *293*, 25-45. https://doi.org/10.1016/j.jvolgeores.2015.01.005

Guinot, B.,. Variation du pôle et de la vitesse de rotation de la Terre. *Traité de Géophysique Interne,* **1,** 1973.

Hagan, M. E., & Forbes, J. M. (2002). Migrating and nonmigrating diurnal tides in the middle and upper atmosphere excited by tropospheric latent heat release. *J. Geophys. Res., Atmospheres*, *107*(D24), ACL-6. https://doi.org/10.1029/2001JD001236

Hamilton, W.L (1973), Tidal cycles of volcanic eruptions: fortnightly to 19 yearly periods. Journal of Geophysical Research, 78(17), 3363-3375.

Heaton, T. H. (1975). Tidal triggering of earthquakes. *Geophys. J. Int.,* 43(2), 307-326.

Holgate, S. J., et al. (2013) New Data Systems and Products at the Permanent Service for Mean Sea Level. *J. Coastal Res.*, 29(3), 493–504. https://doi .org /10.2112/JCOASTRES-D-12-00175.1.

Holm, P. M., et al. (2008). An 40Ar-39Ar study of the Cape Verde hot spot: Temporal evolution in a semistationary plate environment. *J. Geophys. Res., Solid Earth*, *113*(B8). https://doi.org/10.1029/2007JB005339

Jenkins, S. F., Day, S. J., Faria, B. V. E., & Fonseca, J. F. B. D. (2017). Damage from lava flows: insights from the 2014–2015 eruption of Fogo, Cape Verde. *J. Applied Volcanol.*, *6*(1), 6.

Jentzsch, G., et al. (2001). Mayon volcano, Philippines: some insights into stress balance. *J. Volcanol. Geotherm Res.*, *109*(1-3), 205-217. https://doi.org/10.1016/S0377-0273(00)00312-7

Jobert, G., & Coulomb, J., (1973). Traité de géophysique interne, Tome I: sismologie et pesanteur, *Editions Masson*, *125.*

Keszthelyi, L. (1995). A preliminary thermal budget for lava tubes on the Earth and planets. *J. Geophys. Res. Solid Earth*, *100*(B10), 20411-20420.

Lambeck, K., (2005). *The Earth's variable rotation: geophysical causes and consequences*. Cambridge University Press, chap 5, p 73.

Le Mouël, J.-L., et al. (2019a) A solar signature in many climate indices. *J. Geophys. Res., Atmospheres.* 124.5: 2600-2619. https://doi.org/10.1029/2018JD028939

Le Mouël, J. L., et al. (2019b). On forcings of length of day changes: From 9-day to 18.6-year oscillations. *Phys. Earth Planet. Inter.*, *292*, 1-11. https://doi.org/10.1016/j.pepi.2019.04.006

Le Mouël, J. L., Lopes, F., & Courtillot, V., (2020). Characteristic time scales of decadal to centennial changes in global surface temperatures over the past 150 years, *Earth Space Sci.*, *7*(4), https://doi.org/10.1029/2019EA000671.

Leva, C., Rümpker, G., Link, F., & Wölbern, I. (2019). Mantle earthquakes beneath Fogo volcano, Cape Verde: Evidence for subcrustal fracturing induced by magmatic injection. *J. Volcanol. Geotherm. Res.*, 386, 106672. https://doi.org/10.1016/j.jvolgeores.2019.106672

Lopes, F., et al. (2017). The mantle rotation pole position. A solar component. *Comptes Rendus Geoscience*, **349**(**4**), 159-164. https://doi .org /10 .1016 /j .crte .2017.06 .001.

Mata, J., et al. (2017). The 2014–15 eruption and the short-term geochemical evolution of the Fogo volcano (Cape Verde): Evidence for small-scale mantle heterogeneity. *Lithos*, *288*, 91-107. https://doi.org/10.1016/j.lithos.2017.07.001

Mauk, F. J., & Johnston, M.J.S. (1973). On the triggering of volcanic eruptions by Earth tides. *J. Geophys. Res.*, ***78***(**17**), 3356-3362. https://doi .org /10 .1029 /JB078i017p03356

McMillan, T. C., et al. (2019). Utilizing the impact of Earth and atmospheric tides on groundwater systems: A review reveals the future potential. Rev. Geophys., 57(2), 281-315. https://doi .org /10 .1029 /2018RG000630.

Patanè, G., Frasca, A., Agodi, A., & Imposa, S. (1994). Earth tides and Etnean volcanic eruptions: an attempt at correlation of the two phenomena during the 1983, 1985 and 1986 eruptions. Phys. Earth Planet. Inter., 87(1-2), 123-135.

Petrosino, S., Ricco, C., De Lauro, E., Aquino, I., & Falanga, M. (2020). Time evolution of medium and long-period ground tilting at Campi Flegrei caldera. *Adv. Geosci.*, 52, 9–17. https://doi.org/10.5194/adgeo-52-9-2020

Petrosino, S., Cusano, P., & Madonia, P. (2018). Tidal and hydrological periodicities of seismicity reveal new risk scenarios at Campi Flegrei caldera. *Scientific reports*, *8*(1), 13808.

Prata, A. J., et al. (2003). Global, long-term sulphur dioxide measurements from TOVS data: A new tool for studying explosive volcanism and climate. Geophys. *Monogr. Ser. -Americ. Geophys. Union*, *139*, 75-92. https://doi .org /10.1029/139GM05

Ramalho, R. S., et al. (2015). Hazard potential of volcanic flank collapses raised by new megatsunami evidence. *Science advances*, *1*(9), e1500456. https://doi .org /10.1126/sciadv.1500456

Ramalho, R., et al. (2010). Tracers of uplift and subsidence in the Cape Verde Archipelago. *J. Geol. Soci.*, *167*(3), 519-538. https://doi.org/10.1144/0016-76492009-056

Ray, R. D., & Erofeeva, S. Y. (2014). Long-period tidal variations in the length of day. *J. Geophys. Res., Solid Earth*, **119**(**2**), 1498-1509. https://doi .org /10 .1002 /2013JB010830

Realmuto, V. J., et al. (1994). The use of multispectral thermal infrared image data to estimate the sulfur dioxide flux from volcanoes: a case study from Mount Etna, Sicily, July 29, 1986. *J. Geophys. Res., Solid Earth*, *99*(B1), 481-488. https://doi.org/10.1029/93JB02062

Richter, N., et al. (2016). Lava flow hazard at Fogo volcano, Cape Verde, before and after the 2014–2015 eruption. *Nat. Hazards Earth Syst*. 16. https://doi.org/10.5194/nhess-16-1925-2016

Ricco, C., Petrosino, S., Aquino, I., Del Gaudio, C., & Falanga, M. (2019). Some Investigations on a Possible Relationship between Ground Deformation and Seismic Activity at Campi Flegrei and Ischia Volcanic Areas (Southern Italy). *Geosciences*, *9*(5), 222.

Rymer, H., & Brown, G. C. (1984). Periodic gravity changes at Poas volcano, Costa Rica. Nature, 311(5983), 243-245.https://doi.org/10.1038/311243a0

Silva, S., Day, S. J., & Fonseca, J. F. B. D. (1999). Fogo Volcano, Cape Verde Islands: seismicity-derived constraints on the mechanism of the 1995 eruption. *J. Volcanol. Geotherm. Res.*, *94*(1-4), 219-231.

Sottili, G., & Palladino, D. M. (2012). Tidal modulation of eruptive activity at open-vent volcanoes: evidence from Stromboli, Italy. *Terra Nova*, *24*(3), 233-237. https://doi .org /10 .1111 /j .1365 -3121.2012 .01059 .x

Sottili, G., Martino, S., Palladino, D. M., Paciello, A., & Bozzano, F. (2007). Effects of tidal stresses on volcanic activity at Mount Etna, Italy. *Geophys Res Lett*, *34*(1). https://doi .org /10.1029/2006GL028190

Sparks, R. S. J. (1981). Triggering of volcanic eruptions by Earth tides. *Nature*, *290*(5806), 448. https://doi .org /10 .1038 /290448a0.

Thivet, S. et al. (2020). Evidences of plug pressurization enhancing magma fragmentation during the September 2016 basaltic eruption at Piton de la Fournaise (La Réunion Island, France). *Geochem, Geophys, Geosyst*, *21*(2), e2019GC008611.

Torres, P.C., Madeira, J., Silva, L.C., Brum da Silveira, A., Serralheiro, A., Mota Gomes, A., 1998. Carta Geológica das Erupções Históricas da Ilha do Fogo (Cabo Verde): revisão e actualização. Comunicações do Instituto Geológico e Mineiro 84, A193–196.

Vales, D., et al. (2014). Intraplate seismicity across the Cape Verde swell: A contribution from a temporary seismic network. *Tectonophysics*, 636, 325-337.

Varga, P., & Grafarend, E. (2019). Influence of tidal forces on the triggering of seismic events. In *Geodynamics and Earth Tides Observations from Global to Micro Scale* (pp. 55-63). Birkhäuser, Cham.

Vautard, R., Yiou, P., & Ghil, M. (1992). Singular-spectrum analysis: A toolkit for short, noisy chaotic signals. *Physica D: Nonlinear Phenomena*, *58*(1-4), 95-126.

Watson, I. M., et al. (2004). Thermal infrared remote sensing of volcanic emissions using the moderate resolution imaging spectroradiometer. *J. Volcanol. Geotherm. Res.*, *135*(1-2), 75-89. https://doi.org/10.1016/j.jvolgeores.2003.12.017

Williams-Jones, G., et al. (2001). A model of degassing and seismicity at Arenal Volcano, Costa Rica. *J. Volcanol. Geotherm. Res.*,***108*****(1-4**), 121-139. https://doi .org /10 .1016 /S0377 -0273(00)00281 -X.

Zaccagnino, D., et al. (2020). Tidal modulation of plate motions. *Earth-Science Reviews*, 205, 103179. https://doi.org/10.1016/j.earscirev.2020.103179

DATA REFERENCES

Permanent Service for Mean Sea Level (PSMSL). (2019). "Tide Gauge Data", station ID 1914, Extracted from database http://www.psmsl.org/data/obtaining/.

Vieira, G., Mora, C., Pina, P., Ramalho, R., Fernandes, R. (2020). Digital surface model and orthomosaic of the Chã das Caldeiras lava fields (Fogo Island, Cape Verde, December 2016) (Version 1.0.0) [Data set]. Zenodo. http://doi.org/10.5281/zenodo.4035038

FIGURES

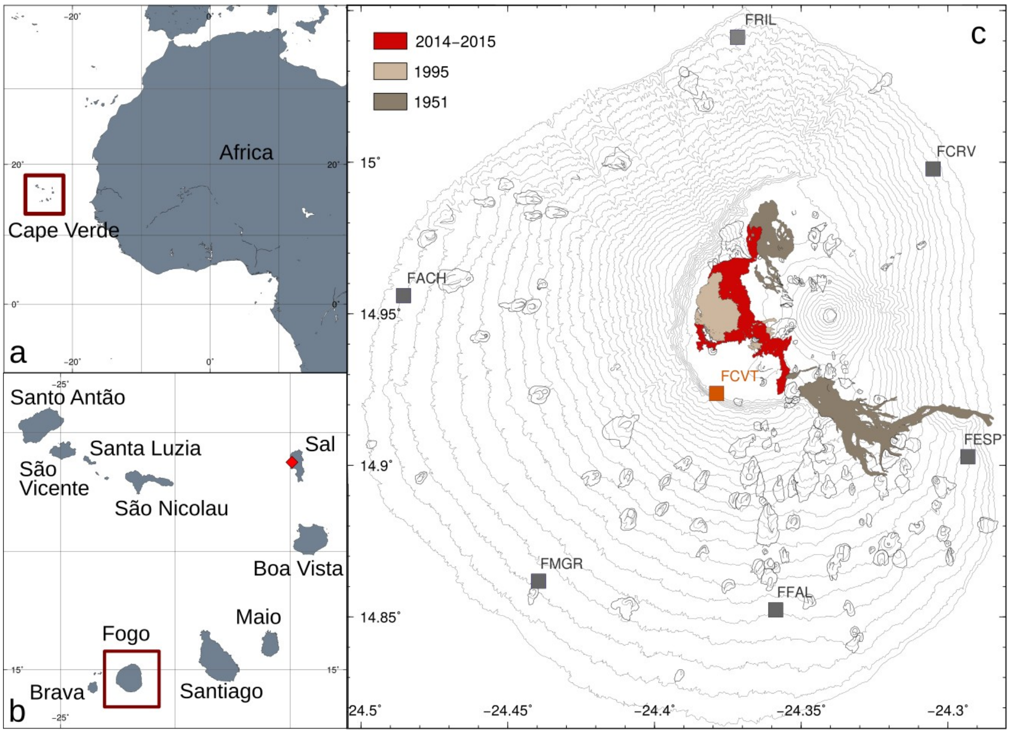

Figure 1: Map of Fogo volcano and the Cape Verde archipelago. Located ~500 km west of the African coast (a), Cape Verde archipelago is composed of a dozen of islands forming a westward-

open crescent (b). Fogo island is located on the southern branch. The red diamond represents the tide gauge where sea level measurements were acquired and used for this study. Fogo island is characterized by a central caldera, Chã das Caldeiras, open to the east (c). Fogo volcano rises nearby the caldera center. The lava fields produced during the last century are represented by the color codes indicated on the upper left of the figure (Torres et al., 1998; Vieira et al., 2020). The topography is represented using 100-m isopachs. The seismic station FCVT (orange square) used in this study was part of a seismic network (gray squares) deployed by the Portuguese government and the C4G consortium during the 2014-2015 eruption.

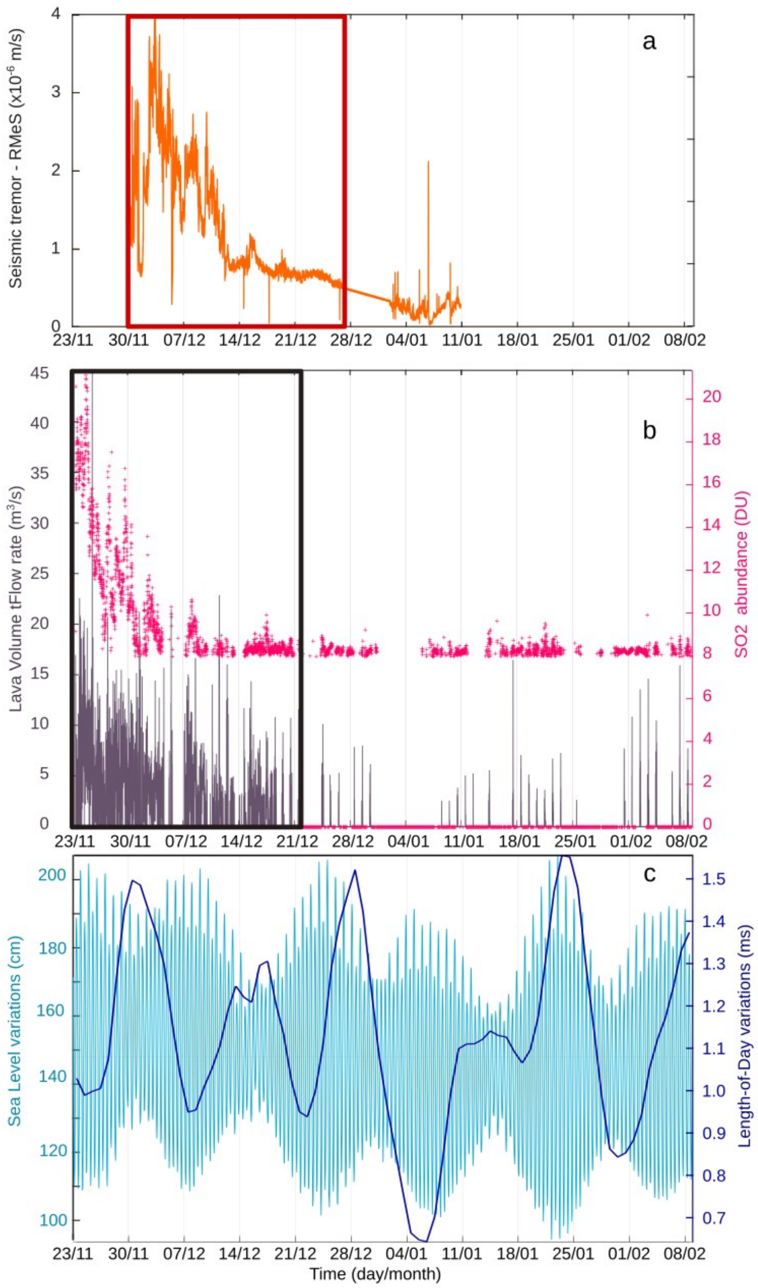

Figure 2: Time-series of the seismic tremor, SO_2 emissions and lava VFR recorded during the 2014-2015 Fogo eruption. (a) Seismic tremor was detected in the 1-4 Hz band at the FCVT station (see Figure 1c for location). (b) SO_2 emission and lava VFR derived from the MSG-SEVIRI satellite data and (c) length-of-day and sea level time-series spanning the whole eruption. The two rectangles indicate the time intervals considered for the present study.

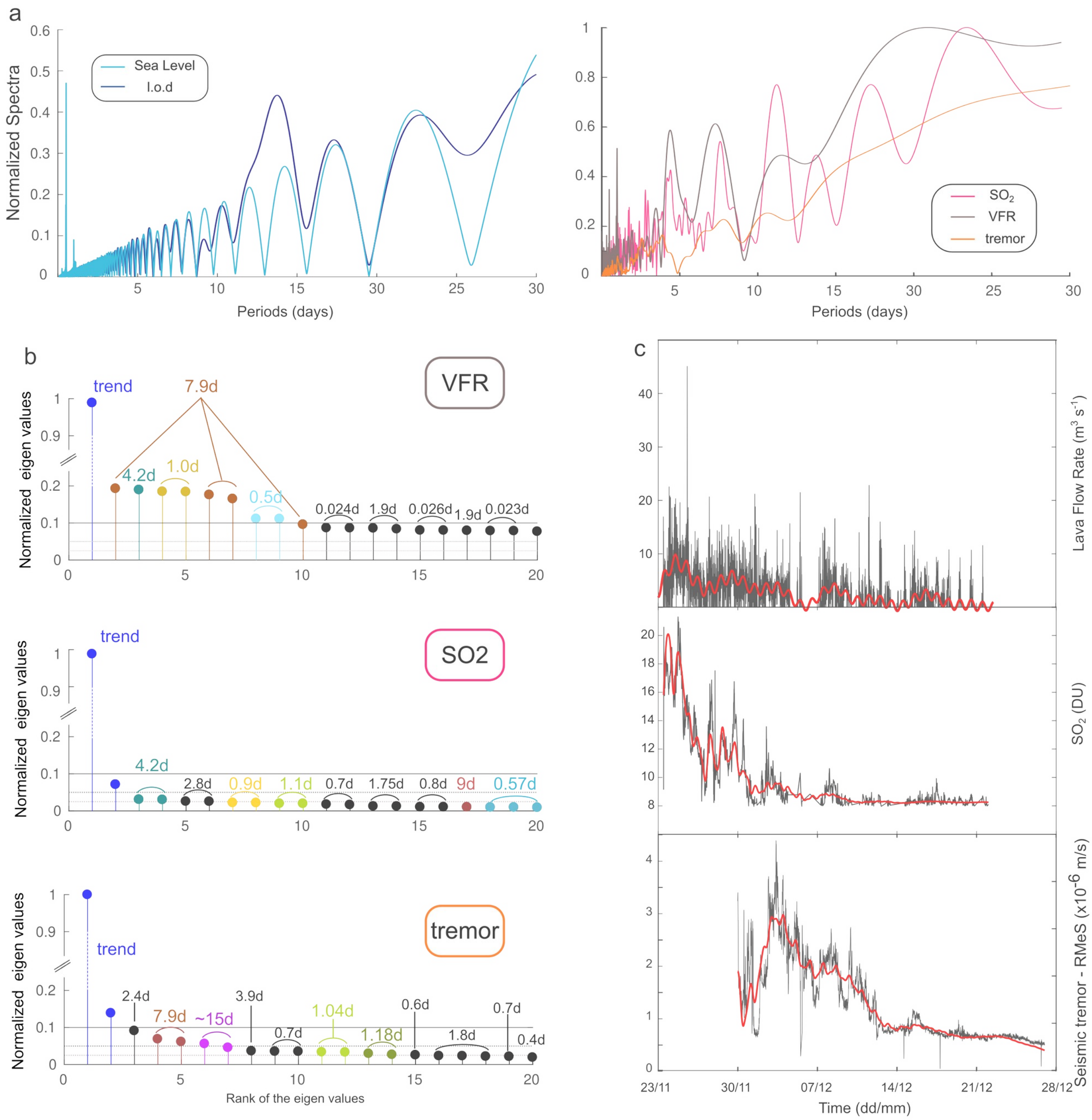

Figure 3: Spectral content and reconstruction of the original volcanological time-series. (a) Normalized spectra of the l.o.d and sea level time-series (left) and for the seismic tremor, SO_2 and

lava VFR time-series (right). (b) Eigen values ranked in decreasing order, are gathered as components representing the trends and (quasi) periodic oscillations of each time volcanological time-series. The different colors correspond to different periodicities identified in the lava VFR, SO_2 and seismic tremor time-series. The black ones were not recognized as main tides and not further considered in this study. (c) Reconstruction (red) of the original time-series (black) of the lava VFR (up), SO_2 (middle) and seismic tremor (bottom) using the trends and the different tidal (pseudo)-periods identified using SSA shown in (b) and listed in Table 1.

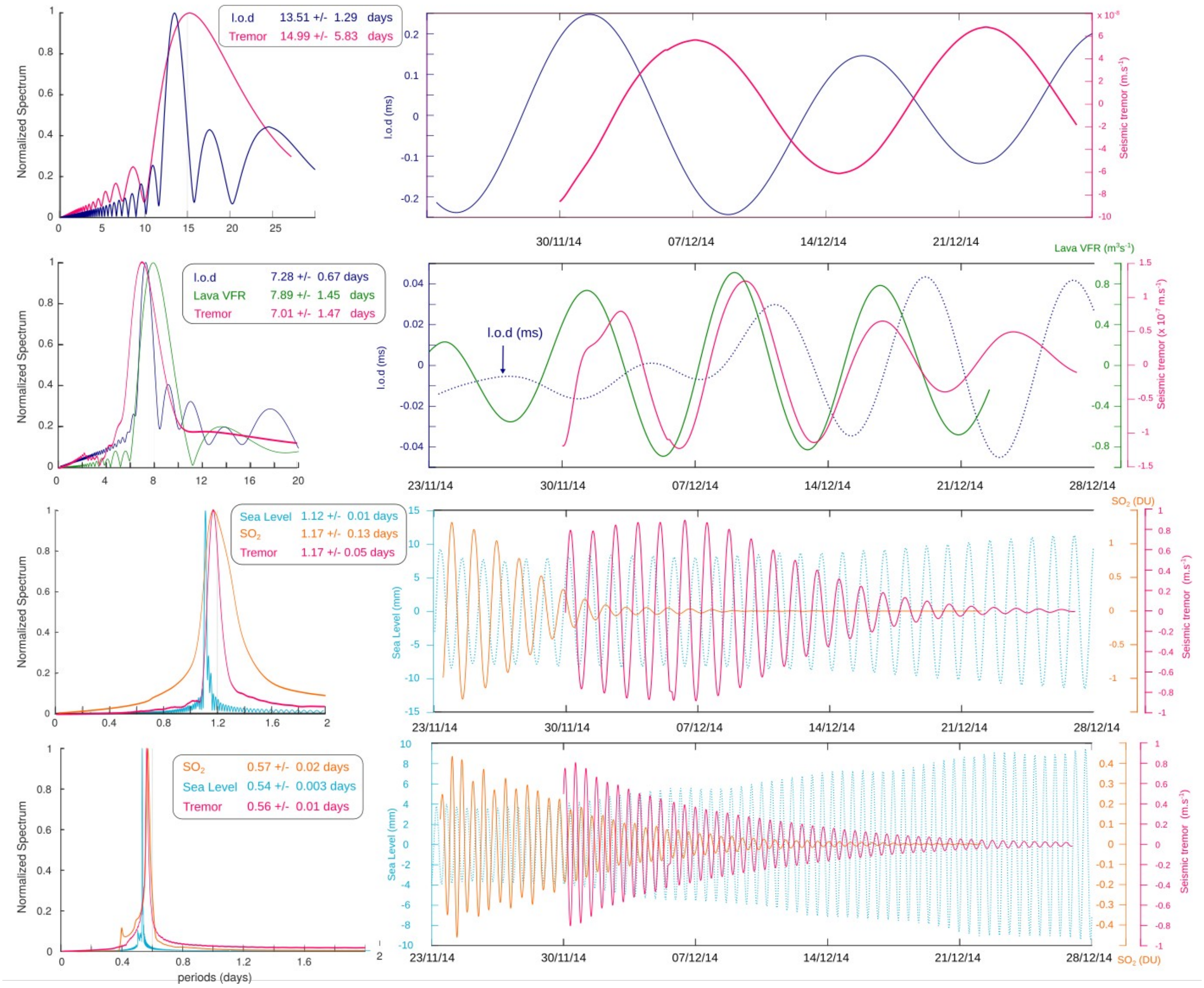

Figure 4: Examples of tidal components extracted in the seismic tremor, SO_2 and lava VFR time-series from ~15 to ~0.5 days (from top to bottom). The normalized spectra are shown on the left side and the corresponding waveforms on the right one. The tidal components of the seismic tremor are represented in pink, those of the SO_2 emission in orange and the lava VFR in green. The components extracted from the l.o.d are in dark blue and in light blue for the sea level, sometimes represented using dotted lines for clarity.

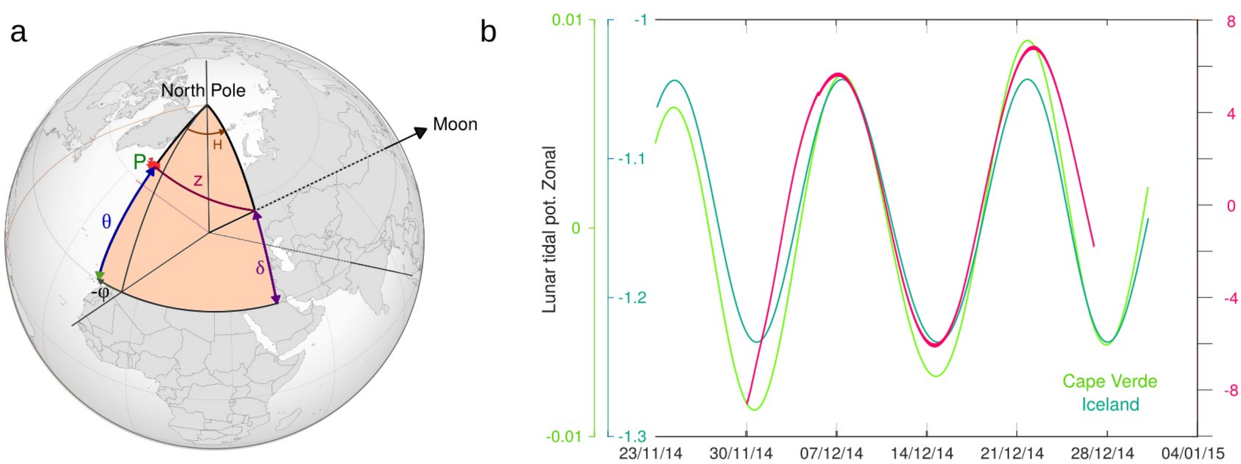

Figure 5: Zonal component of the lunar tidal potential. (a) Parameters used when calculating the tidal potential, depending on the position of the observation site on Earth's planet and that of the celestial body inducing the gravitational force, as the Moon for instance. See Section 3.5 for details. (b) The zonal component due to the Moon gravitational attraction was estimated for two observation sites, Iceland (θ = 65º) and Cape Verde (θ = 15º). These zonal components are compared to the fortnightly component extracted in the seismic tremor at Fogo.

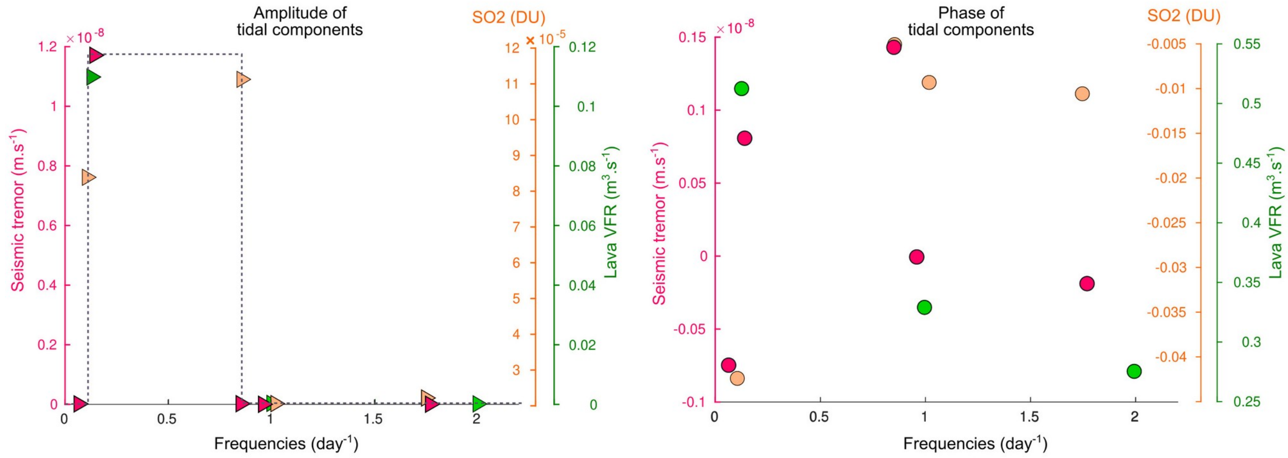

Figure 6: Amplitude and phase associated with all tidal components extracted in the three volcanological time-series during the Fogo eruption, namely seismic tremor (pink), SO_2 emission (orange) and lava VFR (green). The volcano acts as a bandpass filter to tidal components showing sensitivity in the frequency band ~0.1 to 0.85 days^{-1}, and filtering out all other tidal components, as shown by the dotted brown line.

l.o.d (days)	sea level (days)	seismic tremor (days)	lava VFR (days)	SO_2 (days)	Earth tide names	Origin L: Moon; S: Sun
13.51 ± 1.29		14.99 ± 5.8 *(0.07)*			Mf or MSf	L or L+S
9.01 ± 0.57				9.40 ± 2.30 *(0.11)*	Mtm	L
7.28 ± 0.67		7.01 ± 1.5 *(0.14)*	7.89 ± 1.45 *(0.14)*		Mt	L
4.05 ± 0.15*			4.28 ± 0.42*	4.46 ± 0.97*		
	1.12 ± 0.01	1.17 ± 0.05 *(0.85)*		1.17 ± 0.13 *(0.86)*	$2Q_1$	L
	1.08 ± 0.009	1.03 ± 0.1 *(0.96)*			M_1	L
			1.002 ± 0.02 *(1.0)*		P_1	S
	0.999 ± 0.008			0.980 ± 0.06 *(1.02)*	K_1	L + S
	0.54 ± 0.003	0.56 ± 0.01 *(1.78)*		0.57 ± 0.02 *(1.75)*	2"N_2 or N_2	L
			0.50 ± 0.005 *(2.0)*		S_2	S

Table 1: Tidal periodicities identified in the three volcanological time-series, e.g. seismic tremor, lava VFR and SO_2, also extracted in the length-of-day and sea-level variations, used as proxy of the tidal action on Earth. The numbers indicated into brackets in italic are the corresponding frequencies to tidal periodicities in day^{-1}, as represented in Figure 6.